Ann. Occup. Hyg., Vol. 51, No. 2, pp. 189–206, 2007

doi:10.1093/annhyg/mel051

Development and Evaluation of an Air-Curtain Fume Cabinet with Considerations of its Aerodynamics

R. F. HUANG[1]*, Y. D. WU[1], H. D. CHEN[1], C.-C. CHEN[2], C.-W. CHEN[3], C.-P. CHANG[3] and T.-S. SHIH[3,4]

[1]Department of Mechanical Engineering, National Taiwan University of Science and Technology, 43 Keelung Road, Section 4, Taipei, Taiwan, Republic of China; [2]Institute of Occupational Medicine and Industrial Hygiene, National Taiwan University, 1 Jen-Ai Road, Section 1, Taipei, Taiwan, Republic of China; [3]Institute of Occupational Safety and Health, Council of Labor Affairs, Executive Yuan, No. 99, Lane 407, Hengke Road, Shijr City, Taipei County, Taiwan, Republic of China; [4]Graduate Institute of Environmental Health, College of Public Health, China Medical University, 91 Hsueh-Shih Road, Taichung, Taiwan, Republic of China

Received 16 February 2006; in final form 16 June 2006; Published online 20 July 2006

In order to avoid the inherent aerodynamic difficulties of the conventional fume hood, an innovative design—the 'air curtain-isolated fume hood' is developed. The new hood applies a specially designed air curtain (which is generated by a narrow planar jet and a suction slot flow at low velocities) across the sash plane. The hood constructed for the study is full size and transparent for flow visualization. The aerodynamic characteristics are diagnosed by using the laser-light-sheet-assisted smoke flow visualization method. Four characteristic air-curtain flow modes are identified in the domain of jet and suction velocities when the sash remains static. Some of these characteristic flow modes have much improved flow patterns when compared with those of the conventional fume hoods. From the viewpoint of the aerodynamics and mass transport, the results indicate that the air curtain properly setup across the sash opening allows almost no sensible exchange of momentum and mass between the flowfields of the cabinet and the outside environment. Two standard sulfur hexafluoride (SF_6) tracer gas concentration measurement methods following the ANSI/ASHRAE 110-1995 standard and the prEN14175 protocol for static test are employed to examine the contaminant leakage levels. Results of the rigorous examinations of leakage show unusually satisfactory hood performance. The leakage of the tracer gas can approach almost null (<0.001 p.p.m.) if the jet and suction velocities are properly adjusted.

Keywords: air-curtain fume hood; aerodynamic characteristics; fume cupboard; fume hood

INTRODUCTION

Fume hoods are ventilated enclosures used in laboratories where hazardous materials are handled. An exhaust system is connected to the fume hood that draws room air through the hood's sash opening and ejects the mixture of contaminated air out of the laboratory. This enclosure has a movable sash that is positioned to protect the user and allow experiment manipulation. The 'face velocity' (the area-averaged flow velocity across the sash opening) is the first factor considered by the designers for the containment performance of the hood (e.g. Fuller and Etchells, 1979; Caplan and Knutson, 1982; Ivany *et al*., 1989; Fletcher and Johnson, 1992; Maupins and Hitchings, 1998; Volin *et al*., 1998). The back baffle is another factor which drastically influences the distribution of the inlet velocity at the sash opening (Sanders, 1984) and therefore is usually modified by investigators and manufacturers to improve the containment efficiency (Bell *et al*., 2003).

The adjustment of the global flow parameters, i.e. the magnitude and distribution of the face velocity, via the face velocity and back baffle does not guarantee safe extraction of the contaminants (Caplan and Knutson, 1982; Maupins and Hitchings, 1998; First, 2003) because the conventional fume hood is also

*Author to whom correspondence should be addressed.
Tel: +886 2 2737 6488; fax: +886 2 2737 6460;
e-mail: rfhuang@mail.ntust.edu.tw

subject to serious influences of recirculation areas which may be induced around the doorsill, the side poles, interior of the cabinet or area behind the sash, because the interaction occurs inevitably between the flow and the hood structures (Tritton, 1988). Except for the recirculations induced by the flow/hood structure interaction, the presence of the operator may also induce a large recirculation bubble around his chest because the flow drawn into the sash opening goes across the operator's body which can be considered as a situation of bluff-body in cross-flow (Flynn and Ljungqvist, 1995; Guffy *et al*., 2001; Bennett *et al*., 2003). These recirculating vortices may cause the contaminants to be entrained into the separation bubbles and dispersed through the unsteady shear layers to the outer atmosphere via the mechanism of turbulence diffusion. Therefore, some techniques were developed by the investigators to alleviate the vortex-induced spillages of containment, e.g. the by-pass design inside the hood above the sash, the auxiliary air near the face of the hood just above the worker, the doorsill airfoil installation, the doorsill compensation air, the variable air volume (VAV) operation (Ekberg and Melin, 2000), the adaptive back baffle for sash vortex manipulation (the Bi-stable Vortex Fume Hood), the vortex-isolation technique (the Berkeley Hood), etc. The face velocities of the later two strategies may be even lowered down to $\sim$0.3 m s^{-1} while still maintaining good capture efficiency and therefore resulting in apparent energy savings.

Even though the aforementioned techniques proposed by the investigators and manufacturers do improve the containment efficiency, the inherent global and local recirculation flow structures induced by the boundary layer separation or the blockage effect would still inevitably induce more or less turbulent dispersion of the contaminants, particularly when the fume hoods are under the influences of dynamic flow motions. Therefore, the purpose of this article is to provide alternatively an innovative design of fume hood which is based on completely different operation principle from the conventional ones. The flow arrangement and the geometric design are aimed to avoid the induction of the vortical flow structures and build up an effective isolation air curtain to obtain extraordinary low spillage of contaminants. The validation of containment performance of the newly developed fume hood is also reported.

DEVELOPMENT OF AIR CURTAIN-ISOLATED FUME HOOD

It has been known in classical fluid mechanics text books (e.g. Yuan, 1967) that directing a 2D source (e.g. a planar jet) towards a 2D sink (e.g. a suction slot flow) can induce a 2D fluid curtain existing between the source and the sink. This principle has been widely applied in industries which require the removal of contaminant vapors, fumes or aerosols from large open surface during the past half century since Malin (1945) reported that an air curtain set up by the combination of jet and suction flow (push–pull) can save airflow by $\sim$50% when compared with that of using side exhaust alone. Huang *et al*. (2005) proposed a physics-oriented systematic method for design of the push–pull system for large open surfaces. Following proper design rules, the capture efficiency can attain >99% with drastically reduced energy consumption. The laboratory fume hood has a sash opening where the containment may spill off due to the inherent aerodynamic imperfection of configuration design, as discussed previously in the Introduction section. Seeking for an innovative configuration by using the air-curtain isolation concept may provide an approach to avoid the difficulty of the conventional fume hood.

The configuration of the air curtain-isolated fume hood proposed in this study consists of three parts—the sash (structured for supply of push jet with a velocity V_b), the suction slot (installed behind the doorsill for exhaust of contaminants with a suction velocity V_s) and the cabinet (with screens or perforated plates installed on the top), as shown in Fig. 1. The fundamental configurations of the hood are very elementary: no back baffle is present, the doorsill and side poles are not streamlined to meet the aerodynamic requirements (Huang and Lin 1995; Huang and Lee, 2000), no doorsill airfoils are installed and there is no passage to adopt by-pass air. It is just an empty cabinet with special arrangements of push jet and suction slot. The top of the cabinet is covered by mesh screens or perforated plates so that the air is allowed to be drawn into the cabinet by natural convection due to the suction applying at the pull slot. The face velocity of the air drawn from the cabinet top ranges from $\sim$20 to 60 cm s^{-1}, depending on the suction and jet velocities. This natural compensation of air can maintain the pressure in the cabinet at a reasonable level which is a little lower than the atmospheric pressure. For future engineering adaptions the mesh screens or perforated plates can be replaced by various types of mechanical structures. This arrangement is also convenient for the development of a Bio-Safety Cabinet (BSC) in which supply of make-up air through a HEPA filter from the roof of the cabinet is required. To ensure the safety of the cabinet top, in case contaminants are released upward at high momentum, or in case of convective airflow from a heat source, experiments of placing an ejector at a height of 75 cm from the work surface of the cabinet, with the smoke or sulfur hexafluoride (SF_6) released at an upward velocity of 60 cm s^{-1}, were conducted. Comparing with the practical uses of the chemical fume hood, the test conditions are pretty rigorous because the upward fume

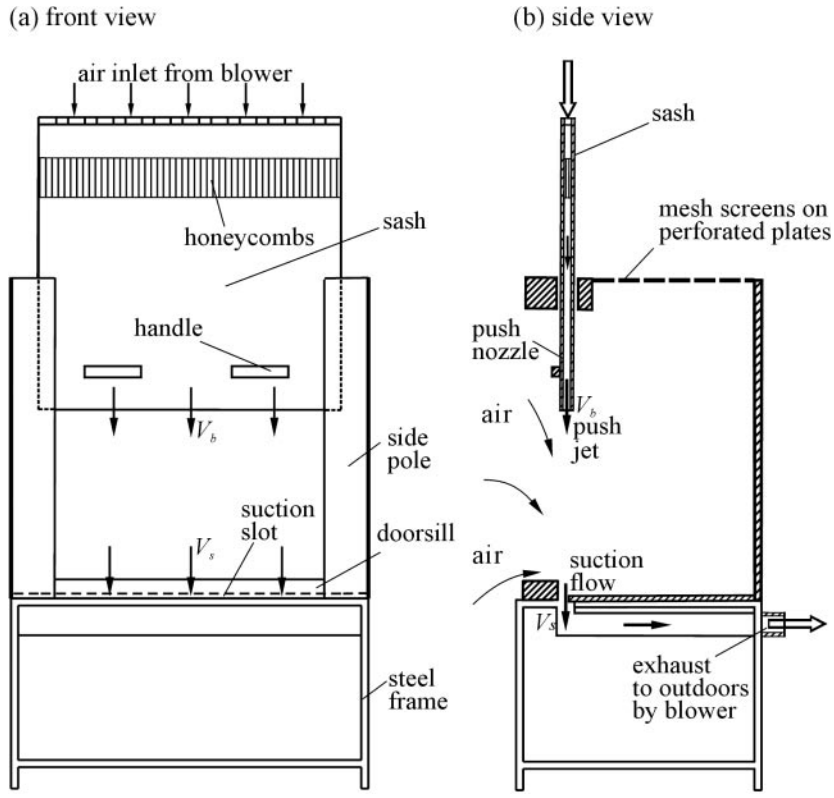

Fig. 1. Arrangement of air-curtain fume hood.

velocity induced by the buoyancy or gas releasing during experiments seldom exceeds 30 cm s^{-1} and the elevation of the fume ejection is usually <60 cm. Neither the smoke nor the SF_6 leakage was detected across the top area.

The push jet and the suction flow are designed to create an air curtain (Huang *et al*., 2005) on the sash plane to aerodynamically separate the interior of the cabinet from the outside atmosphere. The whole fume hood is made of plexiglas which allows the laser-light sheet to penetrate so that flow visualization becomes possible. Honeycombs are inserted into the passages of the sash and the pull hood to improve the uniformity of the jet velocity at the exit of the push nozzle and the suction flow at the opening of the suction hood. The uniformities of the jet and the suction flow are surveyed by a fine wire hot-wire anemometer. The results show that the maximum non-uniformity of the jet and the suction flow are <8%. The push jet and the suction flow are driven separately by centrifugal fans. Inverters are used to control the flow speeds. Venturi flow meters are used to measure the flow rates through the push nozzle and the pull hood. The Venturi flow meters are equipped with high-precision pressure transducers which are constantly calibrated in-house. The accuracy of the flow rate measurement is within the range of 1.5% of converted reading.

The coordinate system and the geometric dimensions are designated in Fig. 2. The hood has a sash opening width of 113 cm. The maximum sash height, which is designated by H_{max}, is 60 cm. The height, width and depth of the cabinet are 132, 148 and 58 cm, respectively. The width at the exit of the sash slot for the push jet during the experiments is varied from 1 to 3 cm, but for the data reported in this paper the width is fixed at 2 cm. The width at the inlet of the suction passage for the experiments is varied from 1 to 4 cm, but for the data reported in this paper the width is fixed at 3 cm. The span of the push jet is 136 cm which is the same as the span of the sash. The span of the suction slot is 145 cm. Therefore the areas of the push jet exit and the suction slot inlet are 272 and 435 cm^2 (0.0272 and 0.0435 m^2), respectively.

MATERIALS AND METHODS

Laser-light sheet flow visualization

The laser beam provided by two 100 mW Nd–Yag lasers are connected to home-made laser-light sheet expanders to obtain laser-light sheets. The laser-light sheet expanders are mounted on adjustable blocks so that the light sheets can be flexibly aimed at any target plane. The laser-light sheets have a thickness of ~0.5 mm. Mineral oil mist is continuously seeded

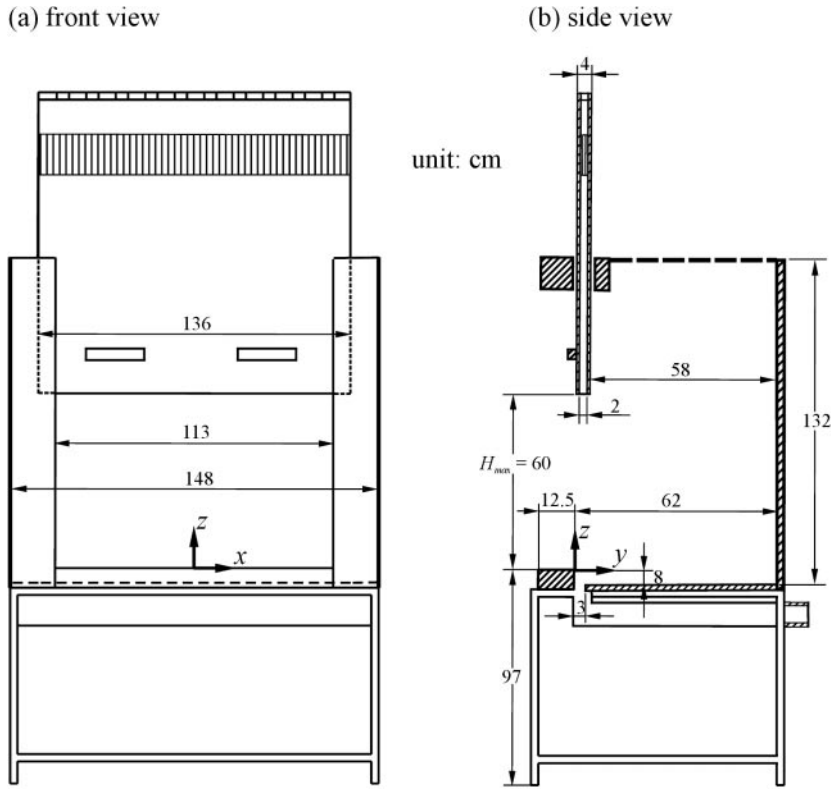

Fig. 2. Dimensions of air-curtain fume hood.

to scatter the laser light via a home-made smoke generator into the push nozzle and/or a standard smoke ejector which are placed in the cabinet and vented out with the pull flow through the suction slot. The diameter of the oil-mist particles, measured by a Malvern 2600C particle analyzer, is 1.7 ± 0.2 μm. The density is 0.821 g ml^{-1}. Ignoring the effect of turbulent diffusion, the relaxation time constant is estimated to be $<7.7 \times 10^{-5}$ s and the Stokes number is in the order of 10^{-6} within the range of experiment. Therefore, the seeding particles can properly follow the flow fluctuations at least up to 10 kHz (Flagan and Seinfeld, 1988). The particle images are recorded by both a Nikon Coolpix 990 digital camera and a HDR-HC1 CCD camera. The digital camera is equipped with an asynchronous variable electronic shutter so that the exposure time can be varied from 0.001 to 8 s. It can take streak pictures at 30 fps (frames per second). The CCD camera can record images at 30 or 60 fps. The exposure time can be varied from 0.0001 to 0.5 s. Because the density of the smoke was not similar to the tracer gases used in the present study, the observed flow patterns of smoke generated as a contaminant inside the cabinet man not be valid for tracer gas generated inside the cabinet. However, the global behaviors of the contaminant moments still can be identified from the streak motions of the smoke flows.

Tracer gas tests

The quantitative containment tests can provide direct information of fume hood performance. Usually, a tracer gas (SF_6) is delivered into the hood cabinet at a known rate and measurements of concentration are collected around the hood to determine gas escape. A pressure gauge, a needle value and a calibrated rotameter are connected to a piping system to control the flow rate of the SF_6 supply.

A number of national standards exist. The ANSI/ASHRAE 110-1995 'Method of Testing Performance of Laboratory Fume Hoods' (ASHRAE, 1995) and prEN 14175-3:2003 'Fume Cupboards Part 3: Type Test Methods' (EN 2003) are employed in this work to diagnose the hood performance and optimize the operation conditions of jet and suction velocities. The ANSI/ASHRAE 110-1995 is focused on the measurement of the SF_6 concentration in the breathing zone of an operator by placing a mannequin in front of the hood. The test methodology of prEN 14175-3:2003 incorporates the inner plane measurement (static sash test), outer plane measurement (sash movement test) and robustness test (walk-bys or gust test). The inner plane measurement was proposed to determine the local average of SF_6 concentration on six sampling regions (each region has an area of 20×20 cm^2) across the sash opening of the fume hood. The inner plane measurement is able to

detect detailed containment leakage in the static sash situation. In this article the results of the static sash test are reported. The ANSI/ASHRAE 110-1995 method uses neat SF_6 as the tracer gas. Since that the injection of high-density gas (such as sulfur hexafluoride) favors vertical stratification with high tracer gas concentrations at bottom of the cabinet (Sandberg and Sjöberg, 1983), the prEN 14175-3:2003 protocol uses 10% SF_6 in N_2 as the tracer gas to reduce the density of the mixture. Besides, because the human body is a heat source with its own convective air flow, such flow therefore may act as a vehicle for contaminants released close to the body (Johnson *et al.*, 1996). Because the ANSI/ASHRAE 110-1995 standard uses non-heated mannequin and does not take the convective air flow into account, the tracer gas data obtained in this paper thus may not be valid for a human being.

Sulfur hexafluoride detector

In the tracer gas experiment, a Miran SapphIRe™ Infrared Analyzer is used to measure the concentration of the SF_6 gas. The instrument is a single beam infrared spectrometer which uses a pyroelectric lithium tantalite substrate as the detector. The lower and upper limits for the detection of SF_6 using this instrument are 0.001 and 100 p.p.m., respectively. The resolution can be set at either 0.01 or 0.001 p.p.m. for display. The instrument is calibrated in-house over four ranges: 0–1, 1–4, 4–24 and values >24 p.p.m.. For concentrations <0.001 p.p.m. and >4 p.p.m., the calibration curves can be used to calculate the values. However, the calculated values lower than 0.001 p.p.m. actually mean 'undetectable' or 'ignorable'. The time constant is 0.05 s. The internal sampling rate of the detector is 20 readings s^{-1}. Average values over 1 or 10 s are recorded in this study (depending on the necessity of experimental conditions) so that the recording data rate is 1 or 0.1 Hz. The inlet diameter and the effective flow rates of the detector probe are 1.3 cm and 14 l min^{-1}, respectively.

Static tests following ANSI/ASHRAE 110-1995 standard

The measurements conducted in accordance with the ANSI/ASHRAE 110-1995 tracer gas containment test method use 100% SF_6 as the tracer gas. Figure 3a and b show the layout and picture, respectively, of the experimental arrangement. The tracer gas ejector is fabricated which follows the test standard. It has a height of 33 cm. The diameters are 13 and 8.5 cm at the screened diffuser and stainless-steel body, respectively. The tracer gas is piped into the ejector inlet and distributed through an outlet of screened diffuser. The flow rate is controlled at 4 l min^{-1} so that the flow velocity out of the screened diffuser is

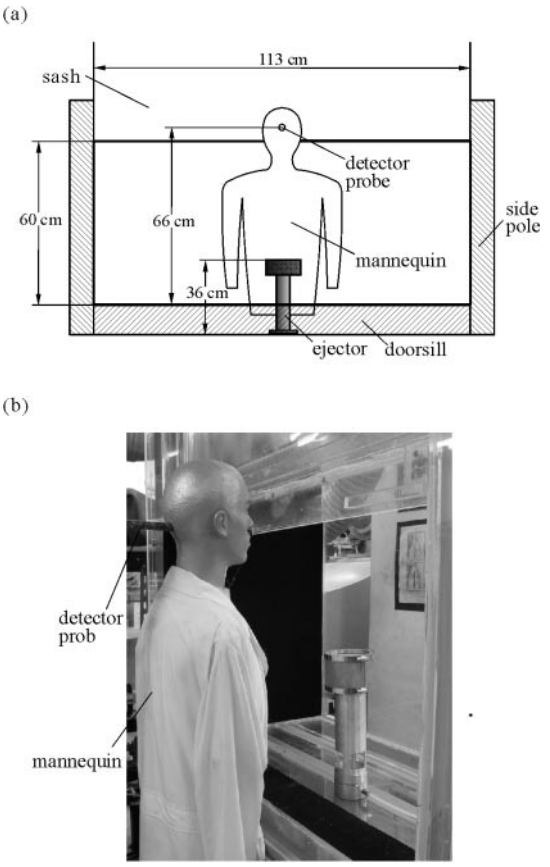

Fig. 3. Deployment of ejector and mannequin following ANSI/ASHRAE 110-1995 Standard. (a) Sketch for relative positions and (b) photo.

$\sim$0.5 cm s^{-1}. The ejector is placed inside the cabinet at positions 15 cm far from the sash plane. A clothed mannequin with a height of 163 cm is used in the experiment. The height and width of its shoulder are 138 and 45 cm, respectively. The mannequin is non-heated. The sampling probe penetrates the head of the mannequin so that the exit of the probe is positioned beneath the nose. The center of the suction inlet of the sampling probe is located 66 cm above the work surface and 7.5 cm away from the sash plane. The tracer gas samples taken from the inlet of the detector probe have a suction velocity of $\sim$175 cm s^{-1}. The arms of the mannequin hang at its sides or penetrate into the cabinet, depending on the experimental situations. When performing experiment, the ejector and the mannequin are simultaneously placed in one of the following three positions: left, central or right position. The ejector centerline has a distance of 30 cm from the left or right lateral walls of the cabinet when the left or right positions are placed. The center position is equidistant from the lateral walls of the cabinet. The SF_6 tracer gas concentration is recorded for a period of 300 s while the tracer gas is released into

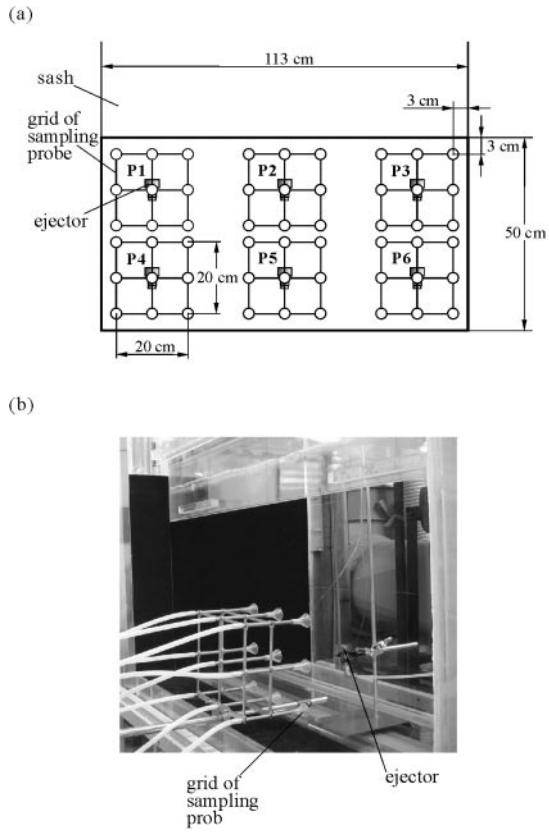

Fig. 4. Deployment of ejector and grid of sampling probes following inner plane measurement method of prEN 14175-3:2003 protocol. (a) Sketch for relative positions and (b) photo.

the cabinet. All the data recorded in the period of 300 s are adopted for the calculation of average value.

Static tests following prEN 14175-3:2003 protocol

The measurements are conducted in accordance with the inner plane measurement method of the prEN 14175-3:2003 protocol by using 10% SF_6 in N_2 as the tracer gas. Figures 4a and b show the layout and picture, respectively, of the experimental arrangement. The tracer gas ejector is a hollow cylinder with a diffusion plate made of sintered metal installed in the ejector. The diameter and length of the ejector cylinder are 1.25 and 2.5 cm, respectively. The release rate of the tracer gas is 2.0 l min^{-1} so that the exit velocity of the ejector is $\sim$27 cm s^{-1}. Nine sampling probes are arranged in a grid based on a square area of 20×20 cm^2. The sampling probes are connected to the inlets of a mixing manifold by Teflon tubes of equal lengths. The detector probe is affixed to the outlet of the mixing manifold. Each sampling probe has a funnel-shaped effuser of 3 cm inner diameter at the inlet. It is fitted to a stainless-steel tube with inner diameter of 0.5 cm and length of 15 cm. The suction velocity at the inlet of the funnel-shaped effuser is $\sim$4 cm s^{-1}. According to the prEN 14175-3:2003 protocol, there are three vertical and three horizontal grid lines separated from each other by 10 cm in both directions. The tracer gas ejector is held vertically up and arranged with its center in-line and 15 cm from the center of the sampling probe grid. The axis of the central probe in the grid is in-line with the mid-point of the ejector. The sampling probe grids are positioned on the sash plane with the center probes at points formed by the intersections of three equally spaced lines between the horizontal boundaries of the sash plane with the two outermost lines 13 cm from the horizontal boundaries. Sampling for the probe-grid positions, as denoted by $\sim$P1–P6 in Fig. 4, is taken sequentially one by one, 360 s for each grid position while the tracer gas is released into the cabinet. The data from the initial period of 59 s is discarded.

Conventional hume hood for comparison

In order to make comparisons, a transparent conventional fume hood with the same frame and sash dimensions as those of the presently developed air-curtain fume hood is fabricated for flow visualization experiment. The conventional fume hood has a suction fan installed on the canopy of the hood cabinet and a back baffle with three rows of slots on the top, middle and bottom for suction of the containment. There is neither by-pass passage nor the airfoil structure arranged on the top of the sash and the doorsill. The face velocity of the conventional fume hood is fixed at 0.5 m s^{-1} in this study.

RESULTS AND DISCUSSION

Characteristic flow modes of air curtain

By using the laser-light sheet flow visualization technique with the assistance of seeding smoke particles into the jet flow as the light scattering media, the flow patterns of the vertical cross-section of the air curtain in the symmetry plane are observed. Figure 5 shows the side-view pictures on the symmetry plane when the camera sees through the lateral transparent wall. The sash and the opening (the sash height set at $H = 60$ cm) are located at the left of the pictures. Four fundamental flow patterns are identified at different values of jet velocity V_b and suction flow velocity V_s.

In Fig. 5a, the jet at a velocity $V_b = 2$ m s^{-1} going out of the sash nozzle deflects a little into the cabinet because the pressure difference exists between the outer environment and the inside cabinet. The jet expands as it goes downstream owing to the entrainment of circumferential air. The jet becomes turbulent with the evolution of shear-layer coherent structures (Schetz, 1980), deflects back to the suction slot (with a

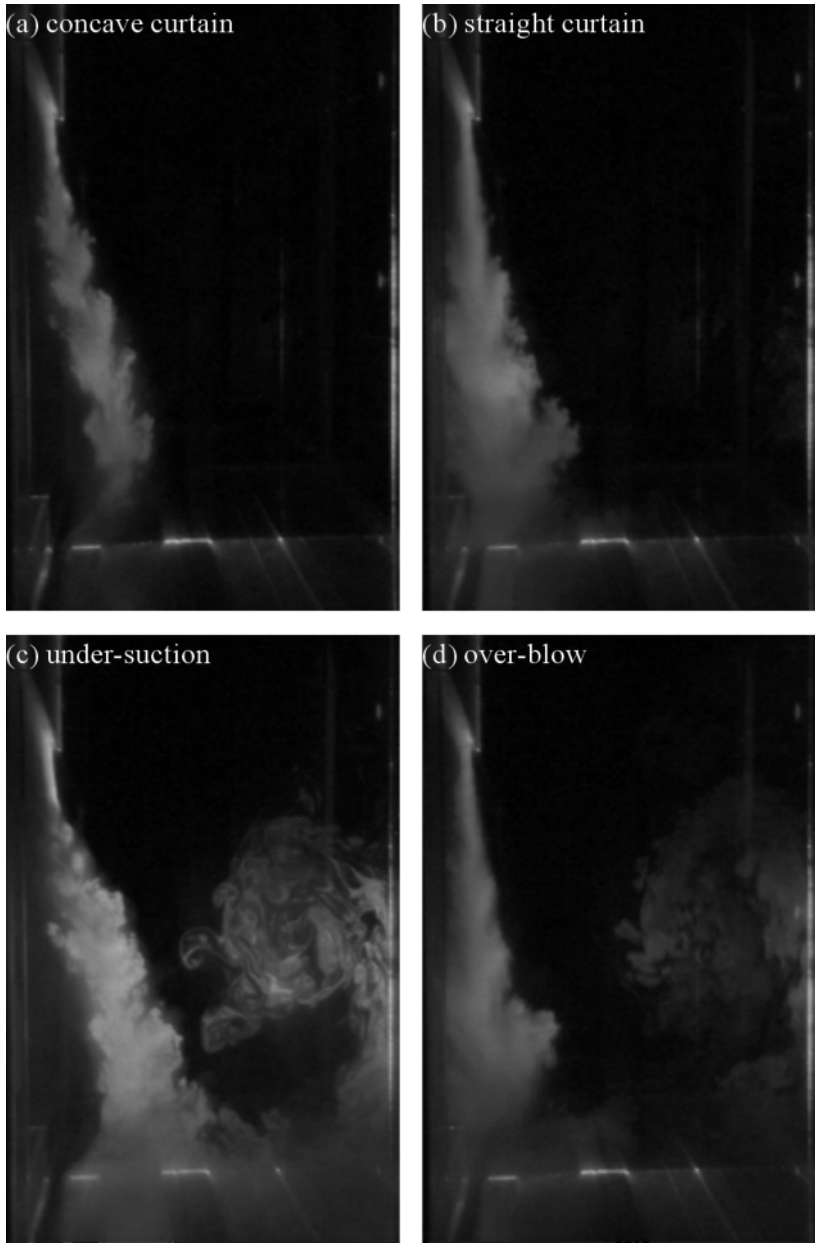

Fig. 5. Photos of typical characteristic flow patterns of air curtain on symmetry plane. Smoke released with jet flow from sash nozzle. Pictures obtained by seeing through the transparent wall of hood cabinet. Sash opening faces left. $H = 60$ cm. (a) 'concave curtain', $V_s = 12$ m s^{-1}, $V_b = 2$ m s^{-1}; (b) 'straight curtain', $V_s = 13.7$ m s^{-1}, $V_b = 4.5$ m s^{-1}; (c) 'under suction', $V_s = 6$ m s^{-1}, $V_b = 1$ m s^{-1}; and (d) 'over-blow', $V_s = 12$ m s^{-1}, $V_b = 6$ m s^{-1}.

suction velocity $V_s = 12$ m s^{-1}) behind the doorsill and subsequently ejects outside the laboratory via the suction blower. When the jet velocity is increased to 4.5 m s^{-1}, as shown in Fig. 5b, the increased jet momentum makes the deflection angle smaller than that observed in Fig. 5a. Although the spatial expansion rate of the jet seems to be increased drastically, all smoke particles seem to still be drawn into the suction slot with the suction velocity of 13.7 m s^{-1}. At low suction velocity, for example, 1 m s^{-1} in Fig. 5c, the jet deflects at a large angle inwards the cabinet, impinges on the cabinet floor and bifurcates into two streams: the small stream is drawn into the suction slot, while the large stream rolls up to form a recirculation vortex in the cabinet. This recirculation vortex grows with the evolution of time and finally occupies about quarter height of the cabinet when the equilibrium is attained. When the jet and the suction velocities are all large (but the increase of suction velocity is not able to catch up the increase of the jet velocity), the major part of the jet fluids is drawn into the suction slot and the minor part of the smoke is

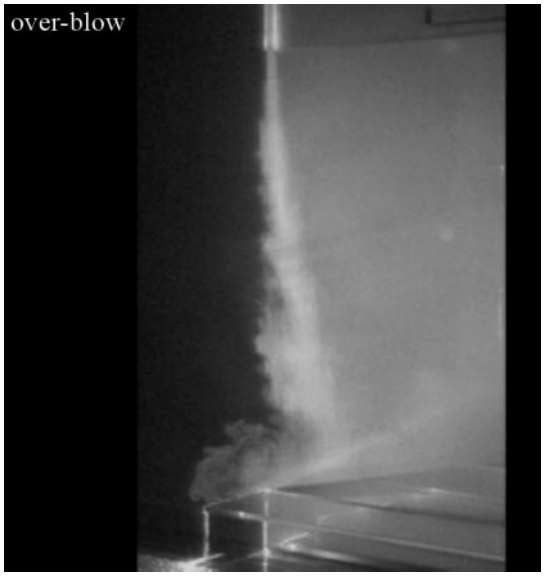

Fig. 6. Flow pattern of 'over- blow' air curtain at $V_s = 3\ m\ s^{-1}$, $V_b = 6\ m\ s^{-1}$. $H = 60$ cm.

diverted to form the in-cabinet vortex, as shown in Fig. 5d. The in-cabinet vortex may eventually occupy about half the height of the cabinet by the time the equilibrium is attained. Because the jet momentum is large, some of the jet fluids are diverted out of the cabinet, impinge on the doorsill, and disperse out to the atmosphere, as shown in Fig. 6.

The flow pattern observed in Fig. 5a is designated as the 'concave curtain' because the jet stream deflects into the cabinet and is drawn through the suction slot. The flow pattern similar to Fig. 5b is termed the 'straight curtain' because the air curtain does not apparently concave inwards and there is an unclear, intermittent small vortex formed on the doorsill. The flow pattern of Fig. 5c is designated 'under suction' because the insufficient suction velocity is supplied and therefore the air curtain concaves inwards severely. The flow pattern corresponding to Fig. 5d is designated 'over-blow' because it features the straight jet, doorsill vortex and large in-cabinet vortex.

The in-cabinet flows are also examined by releasing the smokes through the top screens or perforated plates on the cabinet. The smoke streaks are carried down by the suction currents without causing any reversal for the 'concave curtain' and 'straight curtain' characteristic flow modes. For the 'under suction' and 'over-blow' characteristic flow modes, the smokes are uniformly drawn down before they reach the in-cabinet vortex.

Figure 7 shows the characteristic flow regimes (at the sash height $H = 60$ cm) where the characteristic flow modes discussed above are observed. The bands of short slashed lines represent boundaries between different characteristic flow modes. They are obtained by fixing the jet velocity at various values and increasing the suction flow velocity gradually from zero to high values, and observing the flow patterns directly, by photograph and video. The boundaries are bands rather than lines because the exact positions of the transitions are uncertain. Similar figures (not shown) for sash heights other than 60 cm were also obtained. They all have similar patterns and characteristics. The band separating the regions of 'concave curtain' from 'under suction' moves to lower suction velocity regime as the sash height is decreased, while the boundary band separating the regions of 'under suction' from 'over-blow' does not shift apparently with the change of the sash height.

We now discuss the observed air-curtain flow patterns. The issuing jet initially consists of uncontaminated air, but entrainment may then cause momentum and mass transport between the jet and the circumferential fluids, so further downstream, the jet might have been contaminated by the in-cabinet fluids. The larger the jet momentum is, the higher the entrainment and mixing (Schetz, 1980), and the greater the chance of transverse diffusion of the contaminants across the jet. Therefore, keeping the jet velocity low seems to be an appropriate strategy for the application of the air curtain, if the air-curtain 'strength' for resisting the influences of the cross-drafts or walk-bys of objects is not considered. The flow patterns of 'over-blow' shown in Fig. 5d are obviously not appropriate for the operation of the air curtain because of the induction of large in-cabinet and doorsill vortices which increase the chance of spillage of contaminants. Therefore, operating the air curtain in the flow modes of Fig. 5a–c may be safer than 5d if no outside disturbances are considered. But a strong air curtain is needed to resist the influences of the cross-drafts or walk-bys of objects and, as suggested by Huang *et al.* (2005), increasing the suction velocity while keeping the jet velocity low is an alternative approach of achieving this. It can be argued that for preliminary consideration, operating the fume hood at low jet velocities and in the regime around the boundary between the 'concave curtain' and the 'under suction' modes might be a choice for operation.

Flows around side poles, doorsill and mannequin chest

Flow around side poles. The flow patterns across the vertical cross-sections of the air curtains of the 'concave curtain' and 'over-blow' characteristic flow modes around the left side pole are shown in Fig. 8a and b, respectively. The laser-light sheets in these two figures are positioned vertically immediately to the right of the left side poles. In Fig. 8a, the 'concave curtain' mode, the jet ejected downwards attaches to the inner surface of the side pole due to the Coanda

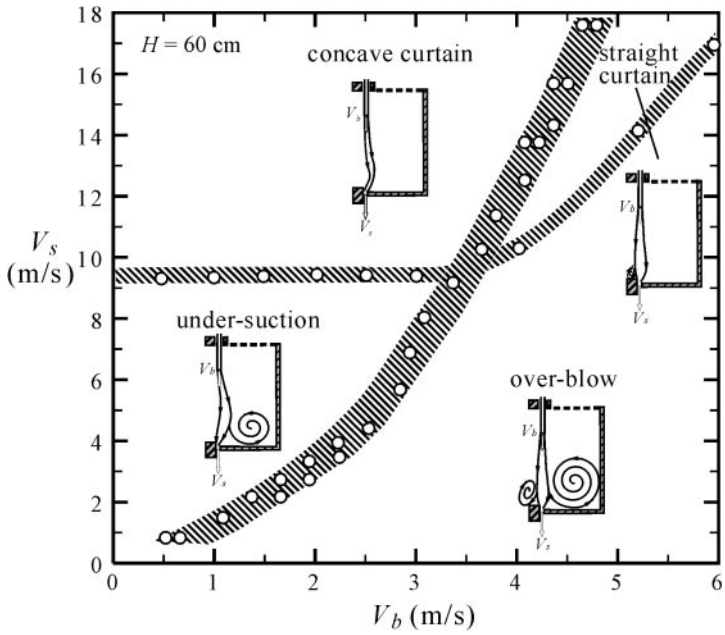

Fig. 7. Characteristic flow regimes of air-curtain fume hood at $H = 60$ cm. Bands of short slashed lines represent boundaries between different characteristic flow modes.

effect (Newman, 1961) to a distance where the jet fluids detach. The detached jet flow curves inwards and is subsequently drawn through the suction slot. Some diverse traces of fluid pockets appear in the mid section near the right surface of the side pole. These fluid pockets are dispersed from the attached air curtain via the recirculation motion of the separated boundary layer existing around the side pole. In the lower section of the side pole, no smoke was observed because the air curtain curves inward. The negative effect of the dispersion of the attached air curtain may not be significant because the smoke is not observed there. Also, because the insignificant dispersion occurs in the mid section of the side pole, the transverse diffusion of the contaminants across the attached air curtain may be negligible. In Fig. 8b, the 'over-blow' mode, the situation similar to Fig. 6 is observed. The strong jet momentum causes impingement of jet fluids on the doorsill. The induced eddies and strong turbulence can cause serious problem for containment spillage. Figure 8c shows the flow pattern across the horizontal cross-section of the 'over-blow' characteristic flow modes around the left side pole. The laser-light sheet is positioned across the horizontal plane 10 cm above the doorsill. A separation bubble with the flow structure connected to the air curtain exists there. Combining Fig. 8b and c, it is apparent that the 3D flow structure appearing near the lower corner of the side pole may have significant negative influences on the containment spillage.

Flow around doorsill. The flows on the symmetry plane around the doorsill are shown in Fig. 9. The smokes are released with a smoke tube attached to the front side wall of the doorsill. The outer air is drawn along the doorsill towards the suction slot. In Fig. 9a–c, for characteristic flow modes of 'concave curtain', 'straight curtain' and 'under suction', respectively, when the flow passes over the front corner, separation of the boundary layer occurs. The separated boundary layer subsequently reattaches to the upper surface of the doorsill in a short distance because the vertical velocity component overwhelms the horizontal velocity component there (Tritton, 1988). The reattached boundary layer is then drawn along the doorsill surface down to the suction slot. The doorsill-induced separation bubble in the conventional fume hood usually causes significant problem of containment spillage and requires special resolution using streamlined surface, airfoil installation or even auxiliary air. In the present design, with down suction and air-curtain isolation, it seems that the doorsill separation bubble does not cause a problem of containment dispersion. Extra efforts to alleviate the negative influence of the separation bubble which is induced when the flow passes over the doorsill seem unnecessary. However, in Fig. 9d for the 'over-blow' mode, the separation bubble does not reattach to the doorsill. Considering the situation of Fig. 5, the possibly contaminated jet fluids may interact with the separated boundary layer and diffuse turbulently out to the atmosphere.

Flow around mannequin chest. Figure 10a shows the flow patterns on the vertical plane outside the sash opening between the sash and the mannequin. The

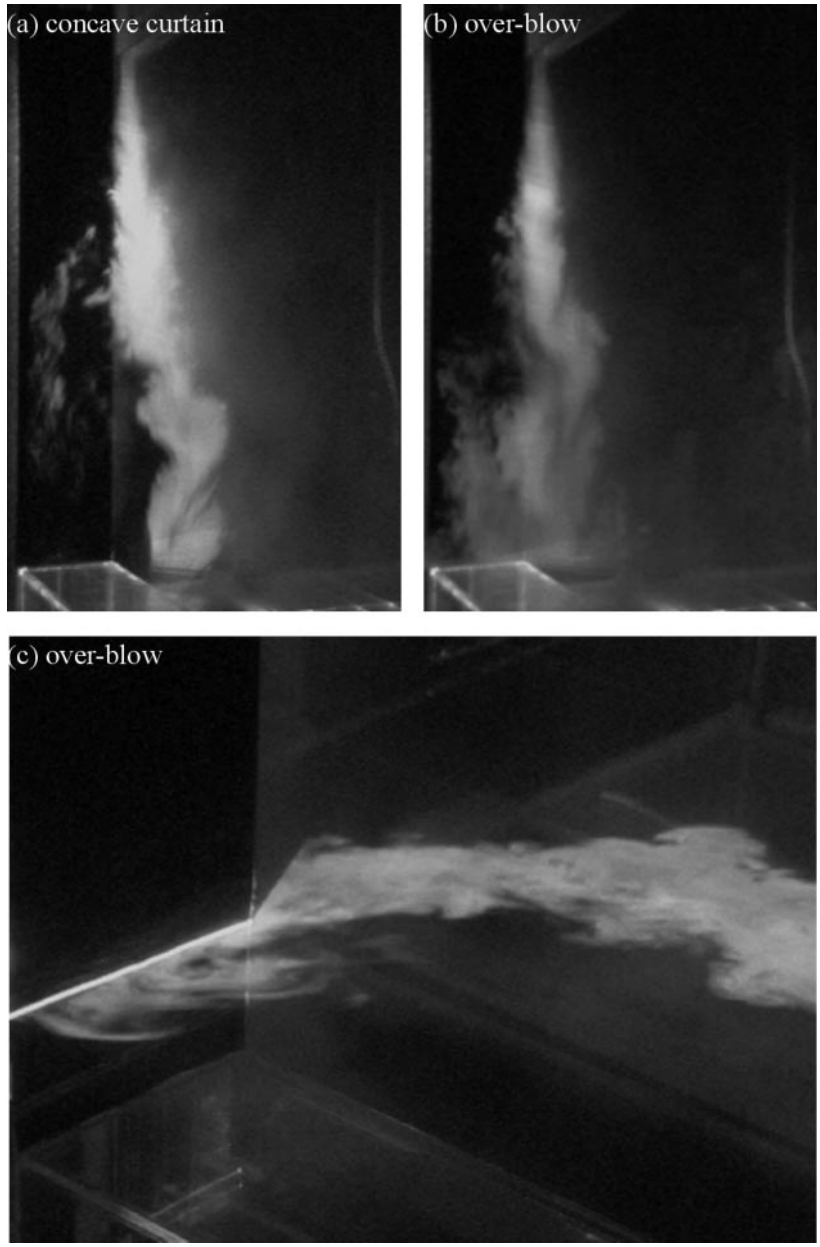

Fig. 8. Flow patterns around left side pole of cabinet. Air-curtain fume hood at $H = 60$ cm. (a) vertical plane, 'concave curtain', $V_s = 12$ m s^{-1}, $V_b = 3$ m s^{-1}; (b) vertical plane, 'over-blow', $V_s = 12$ m s^{-1}, $V_b = 3$ m s^{-1}; and (c) horizontal plane, 'over-blow', $V_s = 12$ m s^{-1}, $V_b = 3$ m s^{-1}.

mannequin is placed in front of the fume hood with the center line on the symmetry plane. The smokes are released via a smoke tube positioned over the head of the mannequin. It is apparent that the streams in this area go directly downward, get across the sash opening and are drawn into the suction slot. No recirculation area is found. By observing the streaklines, the downward velocity component is obviously drastically larger than the horizontal inward velocity component in this area. Therefore, the flow pattern on the horizontal plane across the chest of the mannequin shown in Fig. 10b has a negligibly small recirculation bubble. It is worth mentioning the effect of the human body heat here. According to Johnson *et al*. (1996) and Welling *et al*. (2000), the human body is a heat source and the convective currents at the body are of importance for the breathing zone air quality. Therefore, the visualized flow patterns may not show the exact situations around a human being.

Static tests following ANSI/ASHRAE 110-1995 standard

Figure 11 shows the typical time-evolution records of the SF_6 concentration measured by the detector

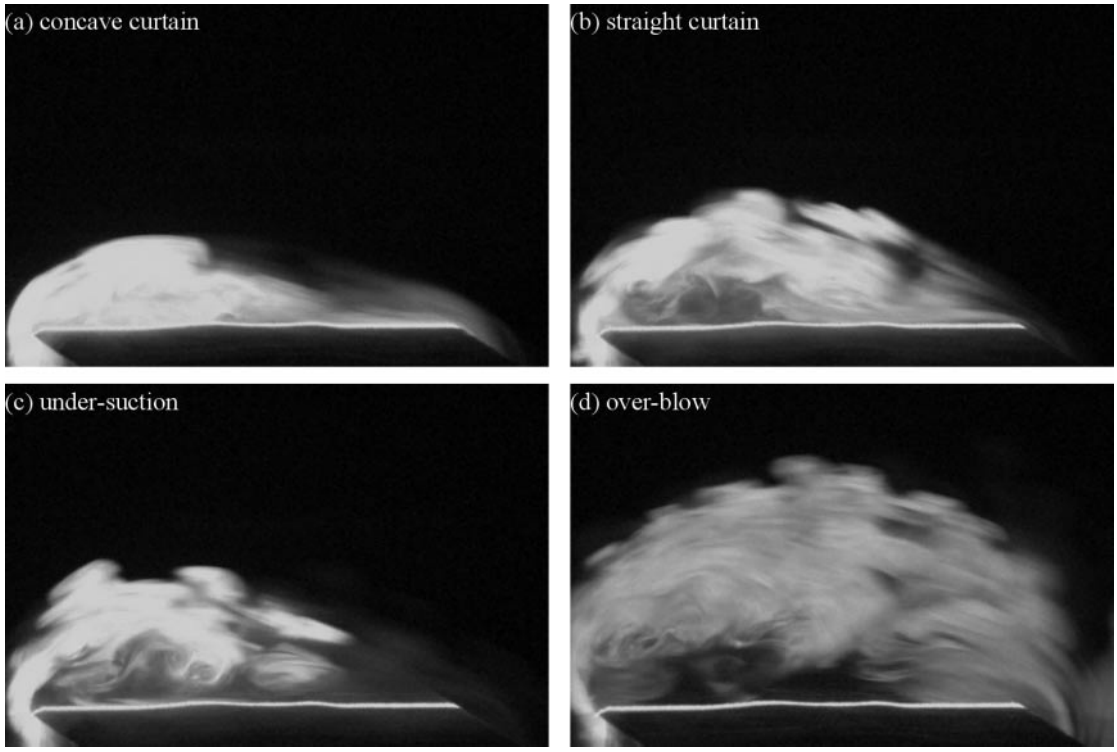

Fig. 9. Flow patterns around doorsill. Air-curtain fume hood at $H = 60$ cm. (a) 'concave curtain', $V_s = 13.7$ m s^{-1}, $V_b = 2$ m s^{-1}; (b) 'straight curtain', $V_s = 13.7$ m s^{-1}, $V_b = 6$ m s^{-1}; (c) 'under suction', $V_s = 6$ m s^{-1}, $V_b = 1$ m s^{-1}; and (d) 'over-blow', $V_s = 6$ m s^{-1}, $V_b = 5$ m s^{-1}.

probe placed under the nose of the mannequin at various combinations of jet and suction velocities when the mannequin is placed at the center position of the hood. The sash height is 60 cm. The levels 0.05 and 0.10 p.p.m. noted by the symbols AM (abbreviation of 'as manufactured') and AI, AU ('as installed', 'as used') in Fig. 11 denote the allowable concentration thresholds set up by the AIHA (2003). The SF_6 concentrations measured in the regimes of 'under suction', 'concave curtain' and 'straight curtain' shown in Fig. 11a–c, respectively, appear to have very low average values <0.001 p.p.m., which is almost undetectable by the Miran SapphIRe^{TM} Infrared Analyzer (the lowest detectable concentration is 0.001 p.p.m.). The variations of SF_6 concentration in Fig. 11a–c are also ignorable because the maximum concentration values in Fig. 11a–c are only 0.001, 0.002 and 0.006 p.p.m., respectively. However, the concentration of SF_6 shown in Fig. 11d for the 'over-blow' flow mode fluctuates drastically and has abnormally large average and maximum values of ~27 and 72 p.p.m., respectively.

Table 1 shows the statistics of the measured average SF_6 concentrations at $H = 60$ and 30 cm. It is interesting that the concentrations measured in the 'under suction', 'concave curtain' and 'straight curtain' regimes are negligible: most of them are <0.002 p.p.m. and few have values of 0.003 p.p.m., which are drastically lower than the AIHA thresholds of AM = 0.05 p.p.m.. Even at $V_b = 0$, where the auxiliary jet is not applied, the detected SF_6 concentrations still remain at the same level as the air curtain-isolated cases. This is because the suction slot is located near the ejector, which is placed at the lower level only 33 cm from the working surface, and the detector probe is placed at the higher level of 66 cm far away from the working surface. This result, however, does not mean that the spillage through the sash opening at other points would be sensitively detected. The concentrations measured in the 'over-blow' characteristic flow mode are all extraordinarily high at both sash heights.

The measured results at the left and right sides of the hood are shown in Table 2. The SF_6 concentrations remain at the same level as that measured at the center. The 3D flow structure appearing near the lower corner of the side pole as shown in Fig. 8 seems not to cause significant containment spillage. The reason may be because that the 3D flow structures existing around the side poles are isolated outside of the cabinet by the air curtain so that the leakage of containment is alleviated.

For comparison, the results of the Berkeley hood (Tschudi *et al*., 2004), the conventional fume hood corresponding to the Berkeley hood, the air-curtain

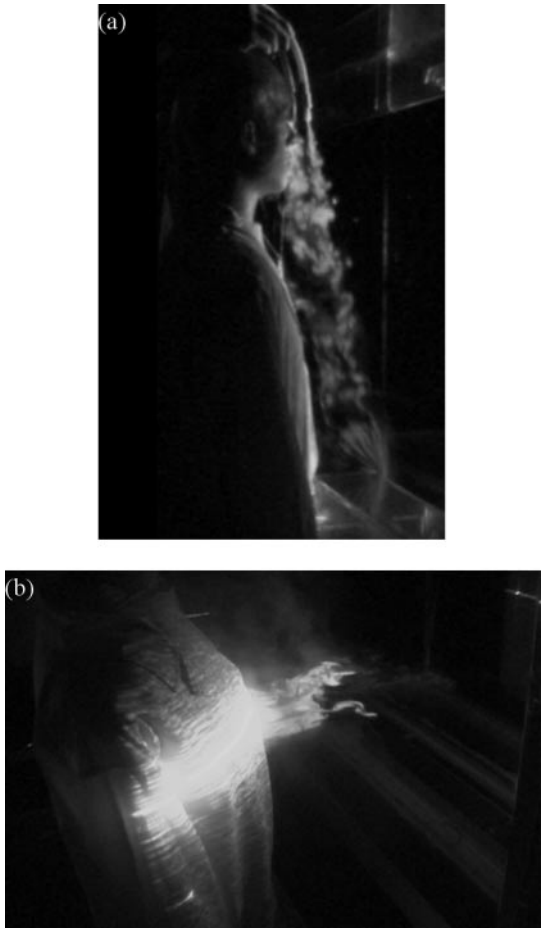

Fig. 10. Flow patterns around chest of mannequin. Air-curtain fume hood at $H = 60$ cm. $V_s = 12$ m s^{-1}, $V_b = 2$ m s^{-1}. (a) Vertical plane and (b) horizontal plane.

hood and the conventional fume hood corresponding to the present air-curtain hood are summarized in Table 3. The data of the Berkeley hood and the conventional hood corresponding to the Berkeley hood are reproduced from Tschudi *et al*. (2004). The tracer gas concentrations listed in Table 3 for four hoods are all far below 0.05 p.p.m. of the AM threshold proposed by AIHA. It seems that the conventional hood which does not use the by-pass, airfoil, streamlined doorsill, etc. (e.g. the one used for purpose of comparison in this study) still can attain a containment spillage much less than the AM threshold, although their leakage level is higher than the modified ones. The concentration levels of the Berkeley hood are much improved when compared with its corresponding conventional hood and the conventional hood corresponding to the present air-curtain hood. The concentration levels of the present air curtain-isolated hood are about the same levels as the Berkeley hood. However, the maximum concentrations measured in the Berkeley hood and the conventional fume hood corresponding to the Berkeley hood, seem to be larger than those of the air-curtain hood.

Table 4 shows the measured SF_6 concentrations of the air-curtain hood when the lower arms of the mannequin are inserted horizontally into the cabinet. The data do not show any particular difference from those obtained in Tables 1 and 2. When operating the air-curtain hood in the regimes of 'under suction', 'concave curtain' and 'straight curtain' characteristic flow modes, the presence of the arms of the mannequin in the cabinet does not change the results of the tests with mannequin's arms hanging to the side and downwards.

Static tests following prEN 14175-3:2003 protocol

As discussed in the Introduction, the shear layers along the separated boundary layers and the vortical flow structures existing around the peripherals of the sash opening are the most critical sources of mass and momentum exchange with the outer environment. The strategy of the inner plane measurement method of the prEN 14175-3:2003 protocol is quite different from that of the ANSI/ASHRAE 110-1995 Standard which emphasizes detection in the hood operator's breathing zone. The prEN is aimed at the detection of hood leakage in local areas covering the whole sash opening so that the most critical areas for containment leakage are included.

The time-evolving SF_6 concentrations of the air-curtain hood at $H = 50$ cm, $V_s = 6$ m s^{-1} and $V_b = 1$ m s^{-1} recorded following the prEN 14175-3:2003 protocol are shown in Fig. 12. The measured instantaneous values at all grid positions do not fluctuate drastically, and the average and maximum values are relatively low. The average and maximum SF_6 concentration values measured for the operation conditions of $(V_s, V_b) = (6, 1)$ and $(10, 1)$ m s^{-1} of the air-curtain hood and the conventional hood corresponding to the air-curtain hood are listed in Table 5. The detected average and maximum values of the air-curtain hood are within the limits of 0.001 and 0.003 p.p.m., respectively. The average and maximum values of the conventional hood corresponding to the air-curtain hood are notably larger than those of the air-curtain hood itself: for this conventional hood the average concentration value of the grid positions ~P1–P3 on the upper rows is ~0.05 p.p.m., while the average concentration value of the grid positions ~P4–P6 on the lower rows is ~27 p.p.m.. The measured maximum concentrations are also high because of large fluctuations. Apparently, the containment performance of the air-curtain hood is superior to that of the corresponding conventional hood. Although there are no test data available for the Berkeley hood following the prEN 14175-3:2003 protocol, a reasonable inference can be made from

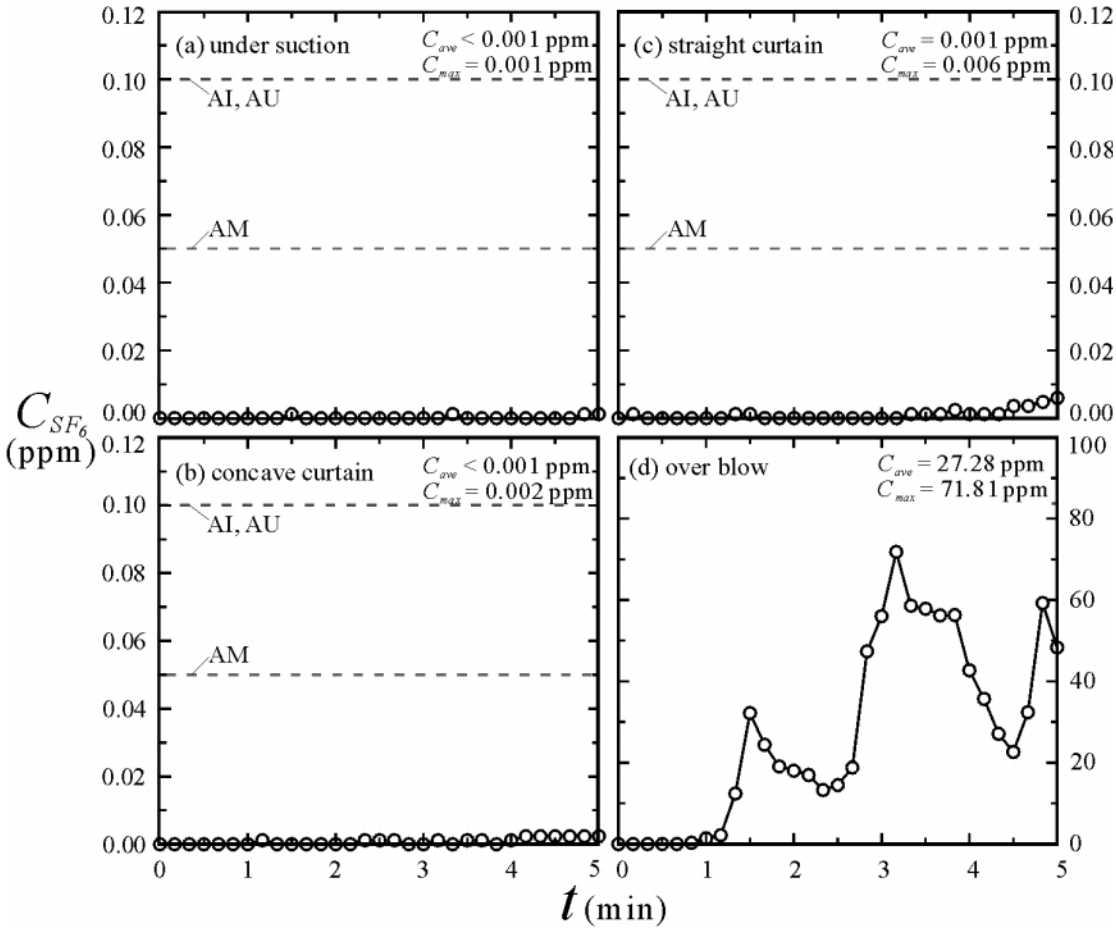

Fig. 11. Measured time-evolving results of SF_6 concentration of air-curtain hood following ANSI/ASHRAE 110-1995 Standard. (V_s, V_b) = (a) (6, 1) m s^{-1}, 'under suction'; (b) (10, 1) m s^{-1}, 'concave curtain'; (c) (12, 4.5) m s^{-1}, 'straight curtain'; and (d) (6, 4.5) m s^{-1}, 'over-blow'.

the test results listed in Table 5 that the vortex-isolation technique employed by the Berkeley hood should reduce containment leakage by isolating the shear layers which are induced by the separated boundary layers evolving from the bottom edge of the sash and the outer edge of the doorsill by using the planar jets issued from the bottom of the sash and the outer edge of the doorsill.

In order to examine the influences of the chest wake with the mannequin present, we conducted experiments using a hybrid method, as shown in Fig. 13. The ejector and the mannequin follow the ANSI/ASHRAE 110-1995 Standard, while the grids of sampling probes follow the prEN 14175-3:2003 Protocol. The tracer gas is 100% SF_6. The flow rate of the ejector is 4 l min^{-1}. The inner diameter of the sampling probe is 2.7 cm. The suction velocity at the inlet of the suction probe is 4.5 cm s^{-1}. The inlets of the sampling probes are on the sash plane. The results of using this hybrid method are shown in Table 6. The measured SF_6 concentrations of the air-curtain hood are not influenced by the presence of the mannequin, consistent with the flow visualization shown in Fig. 10, but with the conventional hood corresponding to the air-curtain hood, the mannequin present gives drastically larger values of SF_6 at P2, P3, P6, P9, P11 and P12 than with the mannequin absent. The potential of containment leakage induced by the mannequin wake and the peripherals of sash opening of the conventional hood is apparently higher than the air-curtain hood.

It is worthwhile to discuss the adequacy of the containment test by using the ANSI/ASHRAE 110-1995 protocol. From the results of the conventional fume hood corresponding to the air-curtain hood listed in Tables 3, 5 and 6, it is obvious that the fume hood which passes the ANSI/ASHRAE 110-1995 test may not pass the prEN 14175-3:2003 protocol because the contaminant leakages may occur in the regions other than the mannequin's breathing zone. Good containment measurement results obtained by following the ANSI/ASHRAE 110-1995 protocol do

Table 1. Results of tracer gas concentration measurements of air-curtain hood

H (cm)	Characteristic flow mode	V_s (m s^{-1})	V_b (m s^{-1})	C_{ave} (p.p.m.)
60	Under suction	1	0	0.002
		3	0	0.001
		3	1	<0.001
		3	1.5	0.001
		6	0	0.001
		6	1	<0.001
		6	2	0.001
		6	3	0.002
		8	0	0.001
	Concave curtain	10	0	<0.001
		10	1	0.001
		10	2	0.001
		10	3	<0.001
		12	1	<0.001
		12	2	0.002
		12	3	0.001
	Straight curtain	12	4	0.001
		12	4.5	0.001
	Over-blow	6	4.5	27
30	Under suction	1	0	0.001
		1	0.7	0.001
	Concave curtain	3	0	0.003
		6	0	0.001
		6	1	<0.001
		6	2	0.001
		8	0	0.002
		10	0	0.003
		10	1	0.001
		10	2	0.001
		10	3	0.001
		12	1	0.003
		12	2	0.001
		12	3	<0.001
	Straight curtain	8	4	0.001
		8	4.5	0.001
	Over-blow	2	4.5	>100

Measurements taken following ANSI/ASHRAE 110-1995 standard. Mannequin and ejector at center positions.

Table 2. Results of tracer gas concentration measurements of air-curtain hood

Test position	H (cm)	Characteristic flow mode	V_s (m s^{-1})	V_b (m s^{-1})	C_{ave} (p.p.m.)
Left	60	Under suction	1	0	0.001
			3	0	0.002
			6	0	0.001
			6	1	<0.001
			6	2	0.001
			8	0	<0.001
		Concave curtain	10	0	<0.001
			10	1	0.003
			10	2	0.001
			10	3	0.001
	30	Under suction	1	0	0.002
			1	0.7	<0.001
		Concave curtain	3	0	<0.001
			6	1	0.002
			6	2	0.001
			8	0	0.001
			10	0	0.001
			10	1	<0.001
			10	2	0.003
			10	3	0.002
Right	60	Under suction	1	0	<0.001
			3	0	<0.001
			6	0	<0.001
			6	1	0.002
			6	2	0.001
			8	0	0.001
		Concave curtain	10	0	0.001
			10	1	0.002
			10	2	<0.001
			10	3	0.001
	30	Under suction	1	0	0.003
			1	0.7	0.001
		Concave curtain	3	0	0.001
			6	0	<0.001
			6	1	0.001
			6	2	0.001
			8	0	<0.001
			10	0	0.003
			10	1	<0.001
			10	2	0.002
			10	3	0.003

Measurements taken following ANSI/ASHRAE 110-1995 standard. Mannequin and ejector at left and right positions.

not guarantee the measurements taken at the regions other than the breathing zone being also under the threshold limit. Therefore, the test data derived from the ANSI/ASHRAE 110-1995 protocol may not be adequate for describing the effectiveness of a fume hood.

The flow rate required to generate 5 m s^{-1} of suction velocity is 0.21 m^3 s^{-1}. The total flow rate required to generate 6 m s^{-1} of suction velocity and 1 m s^{-1} of jet velocity is 0.280 m^3 s^{-1}. The suction flow rate of the conventional fume hood used in this experiment is about 0.35 m^3 s^{-1} (which is not exceptional for a commercial high-performance fume hood). The energy consumption by using the air-curtain fume hood is therefore ~20–40% lower than that of the conventional hood and is able to obtain extraordinarily higher containment performance even under the influence of

Table 3. Results of tracer gas concentration measurements

Test position	Berkeley hood		Conventional hood corresponding to Berkeley hood		Air-curtain hood [$(V_s, V_b) = (6, 1)$ m s^{-1}]		Conventional hood corresponding to air-curtain hood	
	C_{ave} (p.p.m.)	C_{max} (p.p.m.)	C_{ave} (p.p.m.)	C_{max} (p.p.m.)	C_{ave} (p.p.m.)	C_{max} (p.p.m.)	C_{ave} (p.p.m.)	C_{max} (p.p.m.)
Center	0.002	0.018	0.008	0.021	<0.001	0.001	0.007	0.022
Left	0.007	0.041*	0.009	0.028	<0.001	0.001	0.009	0.014
Right	0.001	0.012	0.006	0.008	0.002	0.003	0.008	0.013

Tests performed according to ANSI/ASHRAE 110-1995 standard. $H = 60$ cm.
*This value was probably caused by opening of a door (Tschudi *et al*., 2004).

Table 4. Results of tracer gas concentration measurements of air-curtain hood

Grid position	Air-curtain hood				Conventional hood corresponding to air-curtain hood	
	Under suction [$(V_s, V_b) = (6, 1)$ m s^{-1}]		Concave curtain [$(V_s, V_b) = (10, 1)$ m s^{-1}]			
	C_{ave} (p.p.m.)	C_{max} (p.p.m.)	C_{ave} (p.p.m.)	C_{max} (p.p.m.)	C_{ave} (p.p.m.)	C_{max} (p.p.m.)
P1	<0.001	0.001	0.001	0.002	0.021	0.052
P2	<0.001	0.001	<0.001	0.001	0.081	0.151
P3	<0.001	0.002	0.001	0.002	0.032	0.063
P4	<0.001	0.002	0.001	0.003	24	46
P5	<0.001	0.002	<0.001	0.001	27	52
P6	<0.001	0.001	<0.001	0.001	31	44

Measurements taken following ANSI/ASHRAE 110-1995 standard. $H = 60$ cm. Lower arms of Mannequin inserted horizontally into cabinet.

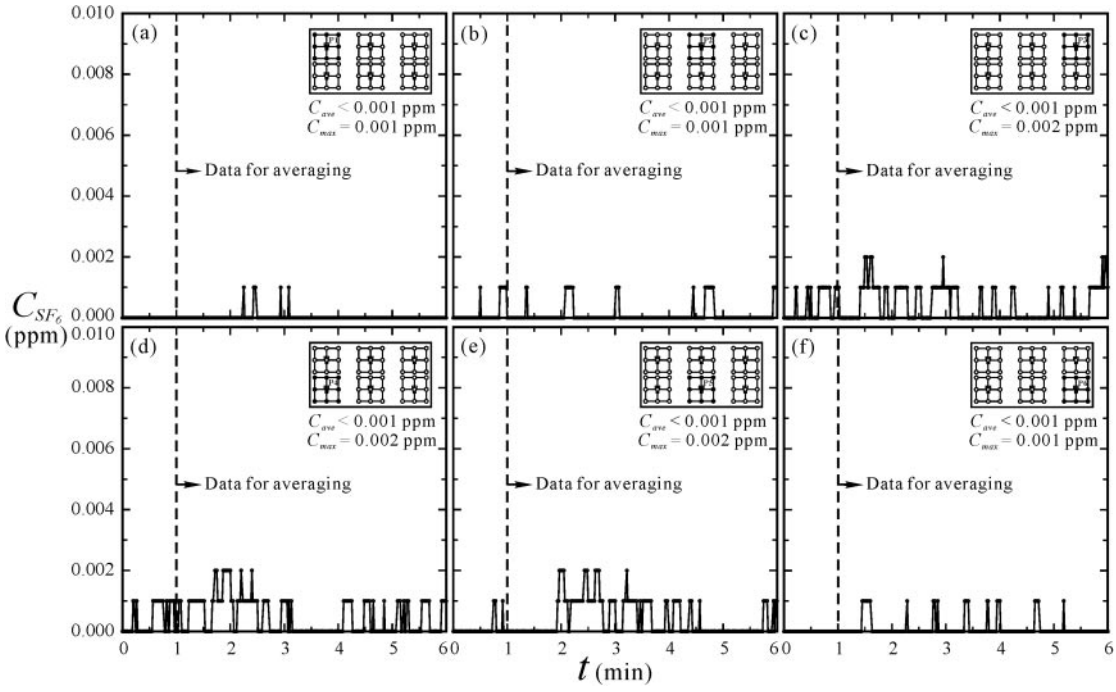

Fig. 12. Measured time-evolving results of SF_6 concentration of air-curtain hood following inner plane measurement of prEN 14175-3:2003 protocol. $(V_s, V_b) = (6, 1)$ m s^{-1}, $H = 50$ cm. Characteristic flow mode is 'under suction'. (a)–(f) are concentrations at the corresponding sampling positions P1–P6 in the inset grids in each chart. (see also Fig 4a).

Table 5. Results of tracer gas concentration measurements following prEN 14175-3:2003 protocol

Grid position	Air-curtain hood (H = 50 cm)		Conventional hood corresponding to air-curtain hood (H = 50 cm)	
	Under suction [(V_s, V_b) = (6, 1) m s^{-1}] C_{ave} (p.p.m.)	Concave curtain [(V_s, V_b) = (10, 3) m s^{-1}] C_{ave} (p.p.m.)	Without mannequin C_{ave} (p.p.m.)	With mannequin C_{ave} (p.p.m.)
P1	0.001	0.002	0.022	0.031
P2	0.001	0.001	0.854	4.662
P3	<0.001	<0.001	1.143	25
P4	<0.001	0.001	0.022	0.020
P5	0.001	<0.001	0.023	0.023
P6	<0.001	0.001	0.011	5.194
P7	0.002	0.001	0.021	0.044
P8	0.002	0.001	0.015	0.011
P9	<0.001	<0.001	0.086	11
P10	0.001	0.001	0.033	0.074
P11	0.001	0.001	18	21
P12	0.001	<0.001	2.550	27

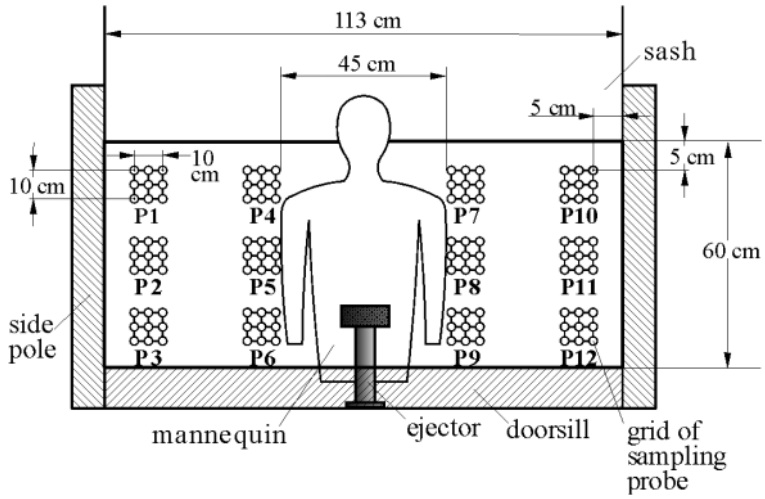

Fig. 13. Deployment of ejector, mannequin, and grid of sampling probes by using hybrid method. H = 50 cm.

environmental drafts. The wider the hood is, the larger the energy saving attained, because the increase rate of the suction flow rate of the conventional fume hood increases faster than the air-curtain hood as the hood width is increased.

CONCLUSIONS

An innovative air curtain-isolated laboratory fume hood is developed. The flow patterns and aerodynamic characteristics associated with the hood are phenomenologically studied. The containment performance of the air curtain-isolated laboratory fume hood is quantitatively validated by measuring the spillage concentration of SF_6 following the ANSI/ASHRAE 110-1995 Standard and the prEN 14175-3:2003 protocol. By properly arranging the jet supply and the suction slot, it is possible to build up an air curtain across the sash opening of a fume hood. The air curtain is expected to isolate the cabinet aerodynamically and to prevent possible loss of cabinet containment, and the downsuction arrangement helps to create this air curtain and provides the exhaust sink. Four characteristic flow modes: 'concave curtain', 'straight curtain', 'under suction' and 'over-blow' are identified according to the aerodynamic characteristics diagnosed by flow visualization technique in the domain of the jet and suction velocities. The 'over-blow' characteristic mode presents a large recirculation vortex in the hood cabinet and on the doorsill, hence operating in that mode is ruled out. The vortices formed around the side poles and the doorsill are connected to the air curtain, instead of the interior containment as in the case of the conventional

Table 6. Results of tracer gas concentration measurements following hybrid method

Test position	Characteristic flow mode (H = 50 cm)	V_s (m s^{-1})	V_b (m s^{-1})	C_{ave} (p.p.m.)
Center	Under suction	1	0	0.001
		3	0	0.002
		3	1.5	0.001
		6	0	<0.001
		6	1	0.001
		6	2	0.001
		6	2.5	<0.001
		8	0	<0.001
	Concave curtain	10	0	<0.001
		10	1	0.003
		10	2	0.001
		10	3	0.003
	Straight curtain	12	4.5	0.002
Left	Under suction	6	1	0.002
		6	2	0.001
	Concave curtain	10	1	0.001
		10	2	0.002
		10	3	0.001

fume hood. Therefore the direct dispersion of the contaminants is alleviated and the necessity of employing streamlined doorsill or airfoil structure is avoided. Owing to the downward flow direction induced by the present arrangement of air curtain, the presence of a mannequin does not induce large recirculation vortex around the chest of the mannequin or create disturbance in the cabinet. When the tracer gas concentration measurements are conducted following the ANSI/ASHRAE 110-1995 Standard and the interior measurement of the prEN 14175-3:2003 protocol for the static sash condition, the average and maximum leakage levels of SF_6 concentrations of the air-curtain fume hood can be in the order of magnitude of 10^{-3} p.p.m. or less even at the low suction velocities, provided the hood is not operated in the regime of 'over-blow'.

Acknowledgement—This research was supported by the Institute of Occupational Safety and Health, Council of Labor Affairs of Taiwan, Republic of China.

APPENDIX

C_{ave} = time-averaged concentration of sulfur hexafluoride.
C_{max} = maximum concentration of sulfur hexafluoride during one sampling period.
H = height of sash opening.
H_{max} = maximum height of sash opening.
Q_b = volumetric flow rate of jet.
Q_s = volumetric flow rate of suction flow.
V_b = area-averaged flow velocity of jet at exit of sash nozzle.
V_s = area-averaged flow velocity of suction flow at inlet of suction slot.
x = coordinate pointing to right side of hood, originated at midway of doorsill.
y = coordinate pointing towards interior of cabinet, originated at inner surface of doorsill.
z = coordinate pointing upwards, originated at upper surface of doorsill.

REFERENCES

AIHA (2003) American National Standard—Laboratory Ventilation. ANSI/AIHA z9.5-2003. Fairfax, VA: American Industrial Hygiene Association. pp. 2–6.

ASHRAE (1995) Method of testing performance of laboratory fume hoods. ANSI/ASHRAE Standard 110-1995. Atlanta, GA: American Society of Heating, Refrigeration and Air Conditioning Engineers Inc.

Bell GC, Sator D, Mills E. (2003) *The Berkeley* hood: development and commercialization of an innovative high-performance laboratory fume hood, Progress Report and Research Status: 1995–2003. Berkeley, CA: Lawrence Berkeley National Laboratory. pp. 3–50.

Bennett JS, Crouch KG, Shulman SA. (2003) Control of wake-induced exposure using an interrupted oscillating jet. Am Ind Hyg Assoc J; 64: 24–29.

Caplan KJ, Knutson GW. (1982) A performance test for laboratory fume hoods. Am Ind Hyg Assoc J; 43: 722–7.

EN (2003) Fume cupboards-Parts 3: type test methods (prEN 14175-3). Brussels: European Committee for Standardization.

Ekberg LE, Melin J. (2000) Required response time for variable air volume fume hood controllers. Ann Occup Hyg; 44: 143–50.

First MW. (2003) Laboratory chemical hoods: a historical perspective. Am Ind Hyg Assoc J; 64: 251–9.

Flagan RC, Seinfeld JH. (1988) Fundamentals of air pollution engineering. Englewood Cliffs, NJ: Prentice Hall. pp. 290–357.

Fletcher B, Johnson AE. (1992) Containment testing of fume cupboards-I, methods. Ann Occup Hyg; 36: 239–52.

Flynn MR, Ljungqvist B. (1995) A review of wake effects on worker exposure. Ann Occup Hyg; 39: 211–21.

Fuller FH, Etchells AW. (1979) The rating of laboratory hood performance. ASHRAE J; 21: 49–53.

Guffey SE, Flanagan ME, van Belle G. (2001) Air sampling at the chest and ear as representative of the breathing zone. Am Ind Hyg Assoc J; 62, 416–27.

Huang RF, Lee HW. (2000) Turbulence effect on frequency characteristics of unsteady motions in wake of wing. AIAA J; 38: 87–94.

Huang RF, Lin CL. (1995) Vortex shedding and shear-layer instability of wing at low-Reynolds numbers. AIAA J; 33: 1398–1401.

Huang RF, Lin SY, Jan SY *et al*. (2005) Aerodynamic characteristics and design guidelines of push–pull ventilation systems. Ann Occup Hyg; 49: 1–15.

Ivany RE, First MW, Diberardinis LJ. (1989) A new method for quantitative, in-use testing of laboratory fume hoods. Am Ind Hyg Assoc J; 50: 275–80.

Johnson AE, Fletcher B, Saunders CJ. (1996) Air movement around a worker in a low-speed flow field. Ann Occup Hyg; 40: 57–64.

Malin BS. (1945) Practical pointers on industrial exhaust system. Heat Vent; 42: 75–82.

Maupins K, Hitchings DT. (1998) Reducing employee exposure potential using the ANSI/ASHRAE 110 method of testing performance of laboratory fume hoods as a diagnostic tool. Am Ind Hyg Assoc J; 59: 133–8.

Newman BG. (1961) The deflection of plane jets by adjacent boundaries—Coanda effect. In Lachmann GV, editor. Boundary layer and flow control—its principles

and application. Vol. 1. New York: Pergamon Press. pp. 232–64.

Sandberg M, Sjöberg M. (1983) The use of moments for assessing air quality in ventilated rooms. Build Environ; 18: 181–97.

Sanders, GT. (1984) A no-cost method of improving fumehood performance. American Laboratory, 10, 102–103.

Schetz JA. (1980) Injection and mixing in turbulent flow. New York: American Institute of Aeronautics and Astronautics. pp. 19–84.

Tritton DJ. (1988) Physical fluid dynamics. New York: Oxford University Press. pp. 139–50.

Tschudi W, Bell GC, Sartor D. (2004) Side-by-side fume hood testing: ASHRAE 110 containment report (LBID-2560). Berkeley, CA: Lawrence Berkeley National Laboratory. pp. 1–28.

Volin CE, Joao RV, Reiman JS *et al*. (1998) Fume hood performance: face velocity variability inconsistent air volume systems. Appl Occup Environ Hyg: 13: 656–62.

Yuan SW. (1967) Foundations of fluid mechanics. Englewood Cliffs, NJ: Prentice Hall. pp. 220–40.

Welling I, Andersson I-M, Rosen G *et al*. (2000) Contaminant dispersion in the vicinity of a worker in a uniform velocity field. Ann Occup Hyg; 44: 219–25.